

# **Contents**

<b>List of figures</b>	<b>II</b>
<b>List of tables</b>	<b>III</b>
<b>1 Introduction</b>	<b>1</b>
<b>2 Theoretical background</b>	<b>2</b>
2.1 Closed and open cylindrical pores . . . . .	2
2.2 Kelvin equation . . . . .	2
2.3 Condensation and evaporation in non ideal pores . . . . .	4
2.3.1 Condensation and evaporation in a closed straight pore . . . . .	4
2.3.2 Condensation and evaporation in a closed funnelled pore . . . . .	4
2.3.3 Condensation and evaporation in an open straight pore . . . . .	4
2.3.4 Condensation and evaporation in an open funnelled pore . . . . .	8
2.4 Blablabla Näherung . . . . .	9
2.4.1 Transmission of Nanoporous Membranes in Empty and Filled State . . . . .	9
2.4.1.1 Transmission of Empty AAM Membrane . . . . .	9
<b>3 Experimental results</b>	<b>11</b>
3.1 Experimental approach . . . . .	11
3.2 Membrane structure analysis . . . . .	14
3.2.1 Isotherm of an open pore membrane . . . . .	14
3.2.2 Isotherm of a closed pore membrane . . . . .	15
3.2.3 Measurement reproducibility . . . . .	17
3.2.4 Inhomogeneities on one wafer . . . . .	19
3.2.5 Defects . . . . .	19
3.3 The problem of pore opening . . . . .	19
3.3.1 Bad open pores . . . . .	19
<b>Bibliography</b>	<b>23</b>

## List of Figures

2.1	.....	3
2.2	Pressure to diameter conversion by KELVIN equation for the parameters $T = 19^\circ\text{C}$ , $\gamma_{T=19^\circ\text{C}}^{\text{hexane}} = 0,018\,605 \frac{\text{N}}{\text{m}}$ and $V_{\text{mol}, T=19^\circ\text{C}}^{\text{hexane}} = 0,130\,53 \frac{\text{L}}{\text{mol}}$ .....	3
2.3	Condensation and evaporation isotherm model of a closed cylindrical pore. (a) corresponds to the mechanisms in a straight pore whereas (b) does for a funnelled one. The corresponding processes inside the pore are illustrated below the isotherm itself. Colors of the arrows between pore states and the respecting pressure range of the graph match. ....	5
2.4	Condensation (a) and evaporation (b) isotherm of a open straight pore. The corresponding processes inside the pore are illustrated below the isotherm itself. Colors of the arrows between pore states and the respecting pressure range of the graph match. ....	6
2.5	Condensation (a) and evaporation (b) isotherm of a open funnelled pore. The corresponding processes inside the pore are illustrated below the isotherm itself. Colors of the arrows between pore states and the respecting pressure range of the graph match. ....	7
2.6	Absorption and desorption isotherm loops for various kinds of cylindrical pores. For the funnelled pores it is $d > d'$ . ....	8
2.7	Using the blabla approximation for the refractive index of a nanoporous medium the transmission in its empty state is computed in section ????. ....	9
3.1	Convention used to assign membrane depending on their position on the wafer. ....	11
3.2	Wafer 295 and 296 processing scheme. While a  signifies a recorded isotherm, the  means MEB pictures have been taken. Red marks pores closed on one end, green pores open on both ends. The processed wafers are immersed in phosphoric acid for $t_{\text{immerse}}$ or floated on for $t_{\text{float}}$ . ....	12
3.3	SEM image of a membran floated on phosphoric acid until the appearance of milky aspects. ....	14
3.4	Measurement results of open pore membrane 296b'. The dashed lines mark the average condensation and evaporation pressures. ....	15
3.5	SEM images of membrane 295g' implying the pores' funnellization. The pores on the solution side (a) show bigger diameters than those on the aluminum side (b). ....	16
3.6	Measurement results of closed pore membrane 296b in comparison to the open pore membrane 296b'. ....	17
3.7	Reproducibility test comparing multiple isotherms measured for the same membrane 292c. ....	17
3.8	Comparison of closed pore membranes of one wafer. (a) compares membranes of wafer 296 while fig. 3.8(b) deals with 295. ....	18
3.9	Comparison of open pore membranes of one wafer. (a) compares membranes of wafer 292 while fig. 3.9(b) deals with 295. ....	20
3.10	Bad open pores illustrated by the comparison of a closed pore isotherm and a open pore isotherm of membrane 294a. ....	21
3.11	SEM image confirming the bad open pores of membrane 294op. ....	22

## List of Tables

- |  |    |
|--|----|
| 3.1 Wafer specifications. The wafers thickness $l_{\text{pore}}$ , floating time $t_{\text{float}}$ of the <i>barrier layer</i> dissolution process and pore diameter dispersion $\Delta d_{\text{pore}}^{\text{MEB}}$ measured by electron beam microscopy are noted. The latter two parameters apply to the open pore membranes of the respective wafer. . . . . | 13 |
|--|----|

# 1 Introduction

The team I conducted my internship in studies condensation and evaporation of helium in different confined materials. During the last 18 months the group focused on nanoporous membranes as a model system of pores of well defined diameters. The goal of these experiments is to measure the dependency of the pressure, at which the condensation and evaporation occur within the pores, on the pore diameters and the temperature relative to the critical temperature and to compare the results to theoretical models. In this respect, the advantage of helium is the ease of changing the temperature in a large range in respect to the critical temperature  $T_c$  (from  $\frac{T_c}{2}$  to  $T_c$ ).

Nanoporous alumina membranes are widely used for ??? (ref). Typically they have a thickness of several tens of micrometers with pores aligned orthogonally to the membrane's surface. At *Institut Néel*, they are synthesized by Laurent Cagnon using an anodization process. The typical pore diameters ranges from 40 nm to 60 nm with an inter pore distance of 100 nm to 120 nm. Smaller diameters are then obtained by using atomic layer deposition (ALD) of alumina.

At *Institut Néel*, the observation of condensation and evaporation makes use of macroscopic techniques which are volumetric isotherm and light scattering measurements. Hereby, the pressure at which condensation and evaporation occurs is averaged over a very large number of pores. Determining the pore diameters from these quantities therefore requires the production of membranes that are as monodisperse as possible.

The used membranes are characterized by two methods. First, absorption and desorption experiments using hexane as a fluid are conducted. The advantage of hexane over helium is that it allows experimenting at room temperature which makes for much faster executable experimentation. Second, reflection electron microscopy (REM) of the pore ends and the membranes' cross sections.

When the author of this text arrived at *Institut Néel* at the beginning of his internship, experiments with several membranes had already revealed that condensation and evaporation occurred over a relatively broad range of pressures revealing a dispersion of pore diameters. This dispersion could be attributed to multiple effects which are the diameter variation along the length of a single pore due to funnellization and corrugations and the distribution of the pores' diameters.

The goals of the internship were then the following:

- Improving and systemizing the evaluation of the recorded isotherm data
- Performing isotherm measurements on many membranes as to confirm the previously reached conclusions statistically
- Comparing the pore diameters extracted from the volumetric measurements to the ones extracted from the REM results
- Improving the fabrication process to reduce the dispersion
- Testing the efficiency of the ALD process as a means to reduce the pore diameters.

Outlines to come..

In the following,

## 2 Theoretical background

### 2.1 Closed and open cylindrical pores

For simplification, in the following, the term *closed pore* will refer to a cylindrical pore that is closed on one end, whereas an *open pore* is open on both ends. Due to production processes, closed funnelled pores are always closed on the small end leaving the end with the larger diameter open.  
ADD IMAGE???

### 2.2 Kelvin equation

Condensation of a fluid in a cylindrical pore occurs at pressures below the saturated vapor pressure  $P_{sv}$ . For relatively large pores, this is dominantly due to the fluid's surface tension. For a curved meniscus, LAPLACE-YOUNG equation implies

$$P_l - P_v = -\gamma \underbrace{\left( \frac{1}{R_1} + \frac{1}{R_2} \right)}_{:=\zeta}$$

with the pressure inside the liquid  $P_l$ , pressure inside the vapor  $P_v$ , surface tension  $\gamma$  and meniscus radii  $R_1, R_2$  which makes  $\zeta$  the meniscus curvature ????. Connecting this with the phase equilibrium

$$\mu_l(P_l) = \mu_v(P_v),$$

where  $\mu_l$  is the chemical potential within the liquid,  $\mu_v$  the one within the vapor, determines the vapor and the liquid pressure. For an incompressible liquid and a perfect vapor the phase equilibrium becomes

$$\begin{aligned}\mu_l(P_l) &= \mu_l(P_{sv}) + V_{mol}^l (P_l - P_{sv}), \\ \mu_v(P_v) &= \mu_v(P_{sv}) + RT \ln \underbrace{\left( \frac{P_v}{P_{sv}} \right)}_{:=P_{rel}},\end{aligned}$$

with the molar volume of the liquid  $V_{mol}^l$ , the ideal gas constant  $R$  and the temperature of the system  $T$ . Using the definition

$$\mu_v(P_{sv}) = \mu_l(P_{sv})$$

yields

$$-\zeta \gamma V_{mol}^l = RT \ln P_{rel}, \quad (2.1)$$

the so called KELVIN equation.  $P_{rel}$  shall be referred to as the relative vapor pressure from here on.

For a perfectly wetting liquid the meniscus in a closed pore the meniscus curvature is

$$\zeta_{sph} = \frac{1}{R_0} + \frac{1}{R_0} = \frac{2}{R_0}$$

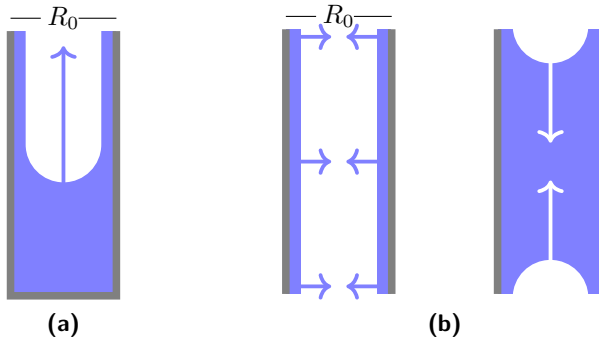


**Figure 2.1**

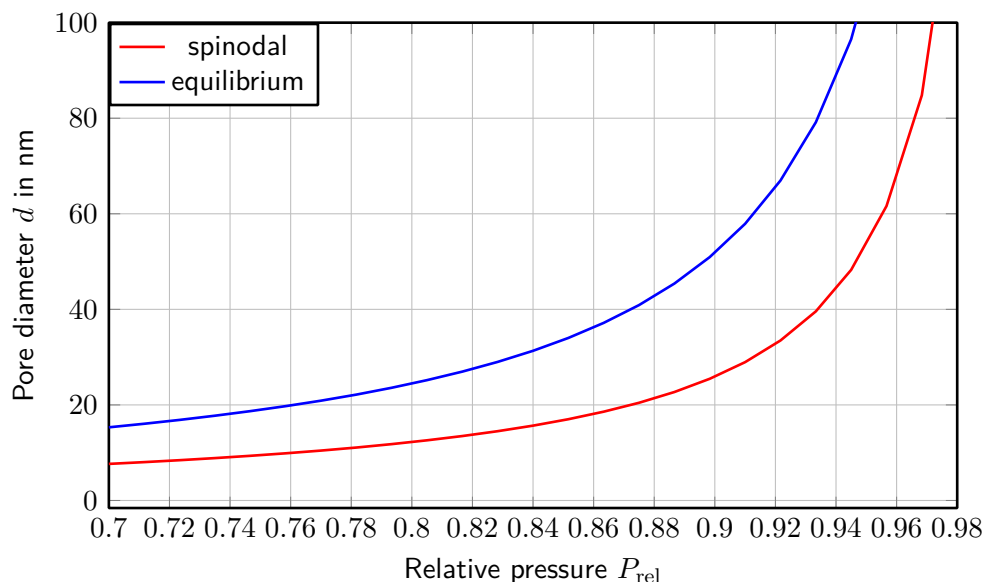


**Figure 2.2** Pressure to diameter conversion by KELVIN equation for the parameters  $T = 19^\circ\text{C}$ ,  $\gamma_{T=19^\circ\text{C}}^{\text{hexane}} = 0,018\,605 \frac{\text{N}}{\text{m}}$  and  $V_{\text{mol}, T=19^\circ\text{C}}^{\text{hexane}} = 0,130\,53 \frac{\text{L}}{\text{mol}}$ .

with the pore diameter  $R_0$ . The result is a shift of the condensation pressure  $P_{\text{cond}}$  from  $P_{\text{sv}}$  to equilibrium pressure

$$P_{\text{eq}} = P_{\text{sv}} \cdot \exp\left(-\frac{2 \cdot \gamma V_{\text{mol}}^1}{R_0 \cdot RT}\right) < P_{\text{sv}}. \quad (2.2)$$

Figure 2.1(a) shows the reversability of the process resulting in the evaporation pressure being

$$P_{\text{evap}} = P_{\text{cond}}.$$

Regarding an open pore - again assuming a perfectly wetting liquid - a hysteresis appears. Unlike for the closed pore, the liquid cannot nucleate from the bottom in this case. In the absence of thermally activated nucleation of a liquid bridge, condensation only occurs due to the collapse of the cylindrical liquid film absorbed on the walls. If the film is much thinner than  $R_1$ , this occurs at the spinodal pressure given by

$$P_{\text{sp}} = P_{\text{sv}} \cdot \exp\left(-\frac{\gamma V_{\text{mol}}^1}{R_0 \cdot RT}\right) < P_{\text{sv}}, \quad (2.3)$$

since the curvature of the menicus is

$$\zeta = \frac{1}{R_0}.$$

The evaporation process that occurs at equilibrium pressure is the same as for the closed pore.

Figure 2.2 shows the relative vapor pressure to diameter conversion for the equilibrium and the spinodal mechanism. The conversion is valid for pores of large diameters in which the thickness of the liquid film is negligible. For smaller pores, where the film's thickness becomes relevant, the theory of SAAM and COLE has to be used rather than KELVIN equation.

Qualatively, the pressures at which condensation and evaporation occur are shifted towards smaller values due to the reduction of the effective pore diameter by the liquid film as shown in ?? (REFHERE???) For even smaller pores, thermal activation may be so important that the hysteresis disappears (REFHERE???).

The long term goal of the team's experiments is to probe these absorption and desorption models. However, for the native pores of 40 nm to 60 nm diameter that are used for the conducted experiments these effects are believed to be small and the KELVIN equation is used to translate the condensation and evaporation pressures to pore diameters.

## **2.3 Condensation and evaporation in non ideal pores**

To understand the condensation and evaporation of hexane in the alumina membranes, the processes must be clear for a single pore. The following explanation starts with a straight cylindrical closed pore. Then, the aspect of funnellization is added to clarify its effect. Moving on to open pores, again, straight pores are followed by funnelled ones.

### **2.3.1 Condensation and evaporation in a closed straight pore**

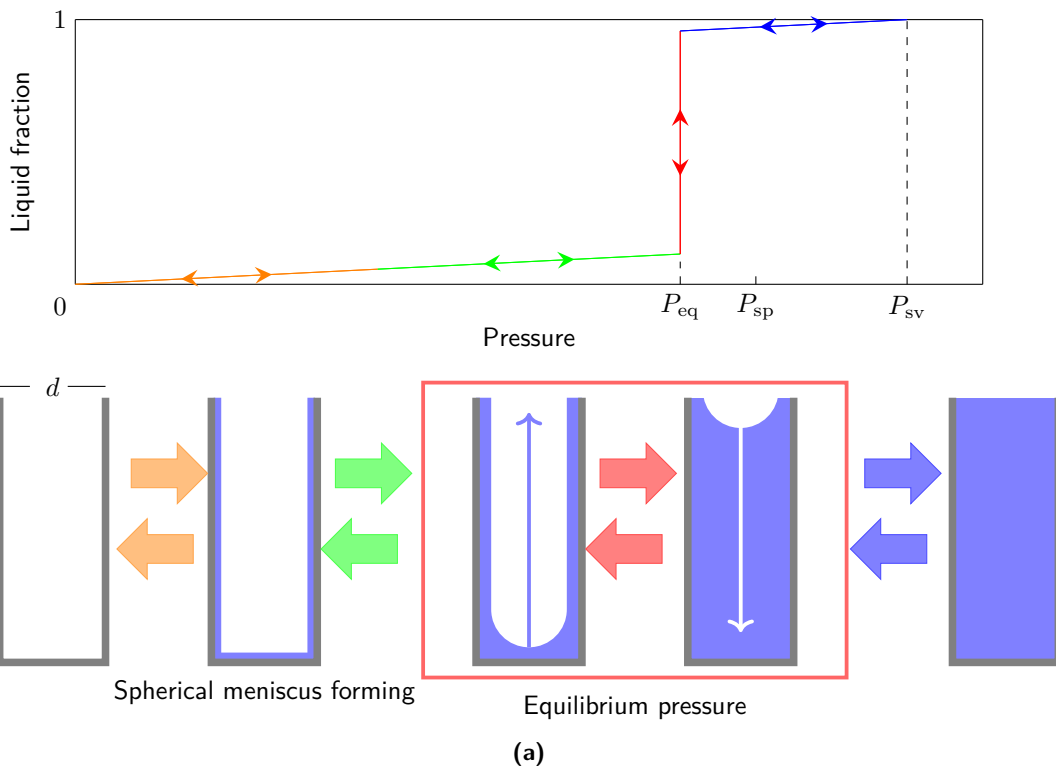
The isotherm of a straight cylindrical pore is illustrated in fig. 2.3(a) with the corresponding processes inside the pore. Exposing the pore to vapor yields a wetting film on its surface (orange pressure range of the isotherm). The film starts forming a spherical meniscus at the closed end of the pore (green). Upon reaching equilibrium pressure  $P_{eq}(d)$  (compare eq. (2.2)) the pore fills, due to the translational symmetry of the meniscus, leaving only a spherical meniscus at the open end (red). The latter evolves with increasing pressure till an even surface is left at saturated vapor pressure  $P_{sv}$  (blue). According to section 2.2, this process is reversible. Upon decreasing the pressure, a spherical menicus forms on the surface of the liquid and recedes to the bottom of the pore at equilibrium pressure. The remaining film evaporates, yielding a fully dried pore at zero pressure.

### **2.3.2 Condensation and evaporation in a closed funnelled pore**

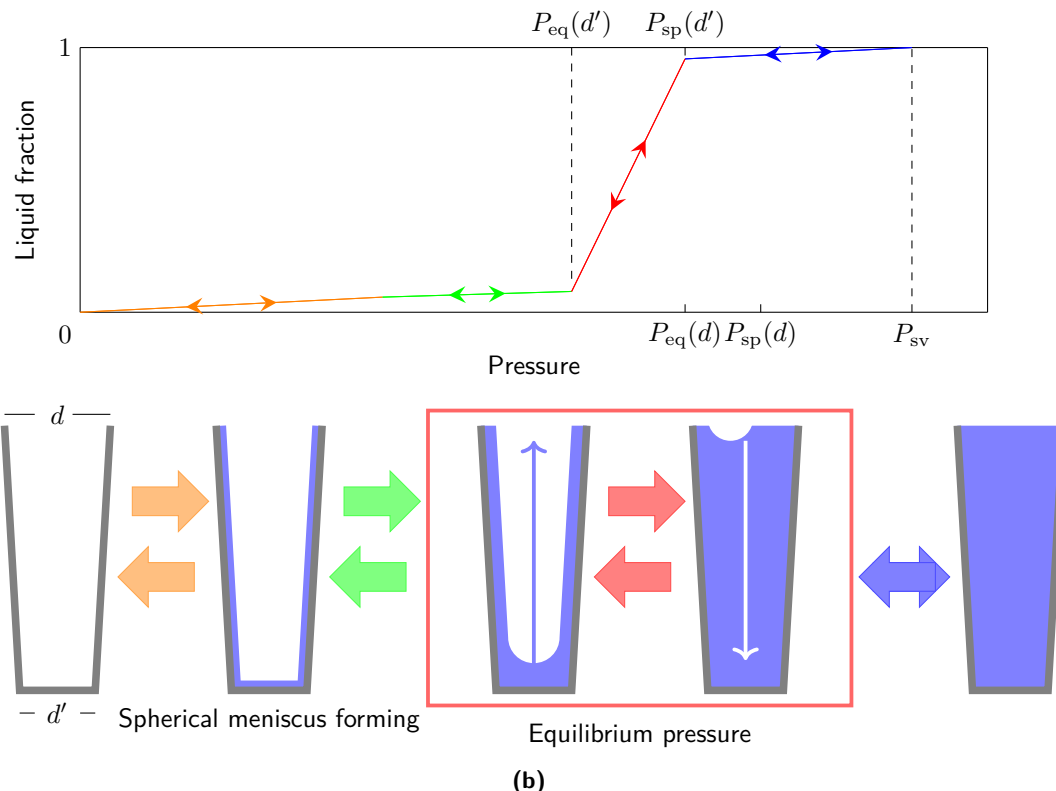
As will be discussed in ???, the membrane production yields funnelled pores which are open on the large end. As in the closed straight pore (section 2.3.1), the condensation and evaporation of liquid in a closed funnelled pore is reversible. The difference is that both processes are continuous now: The pore fills and empties over a pressure range depending on the difference between the pore diameters of the top and bottom side. This makes for an inclined isotherm, as can be seen on fig. 2.3(b).

### **2.3.3 Condensation and evaporation in an open straight pore**

Figure 2.4(a) shows the condensation isotherm branch of an open straight pore and the corresponding processes inside the pore. As explained before, a wetting film forms on the pores inside. However, for an open pore, the latter forms a cylindrical meniscus. Upon reaching the spinodal pressure  $P_{sp}(d)$  (compare eq. (2.3)), the film collapses, yielding a filled pore with menisci at either open end (red).

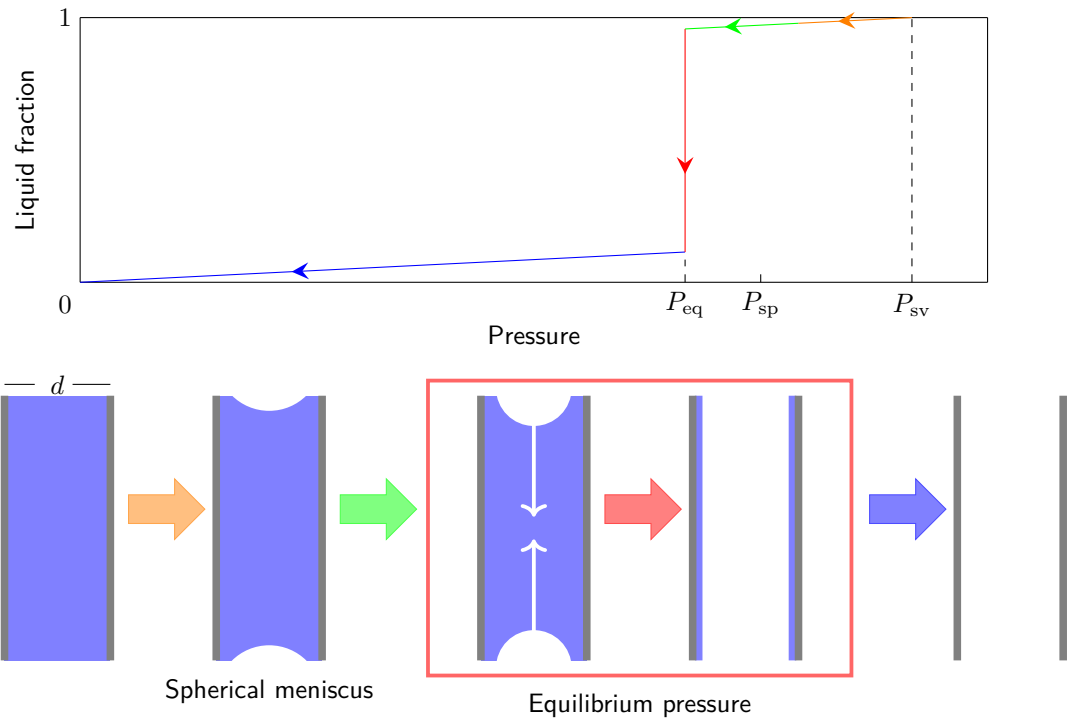
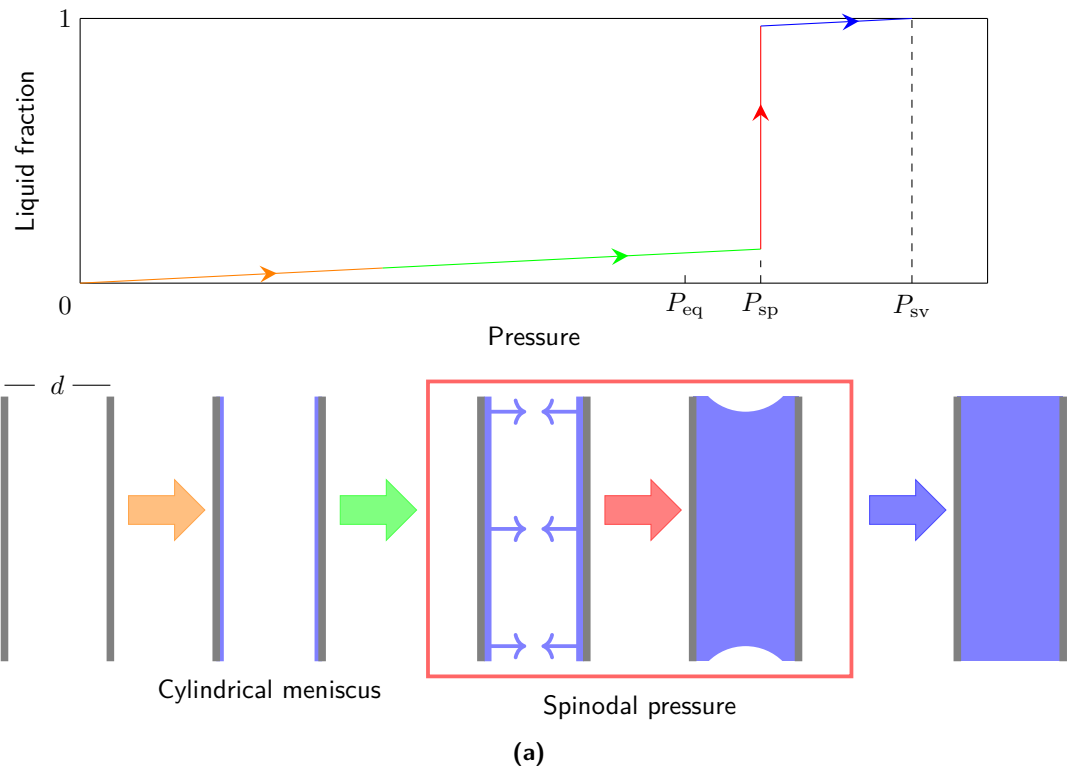


(a)



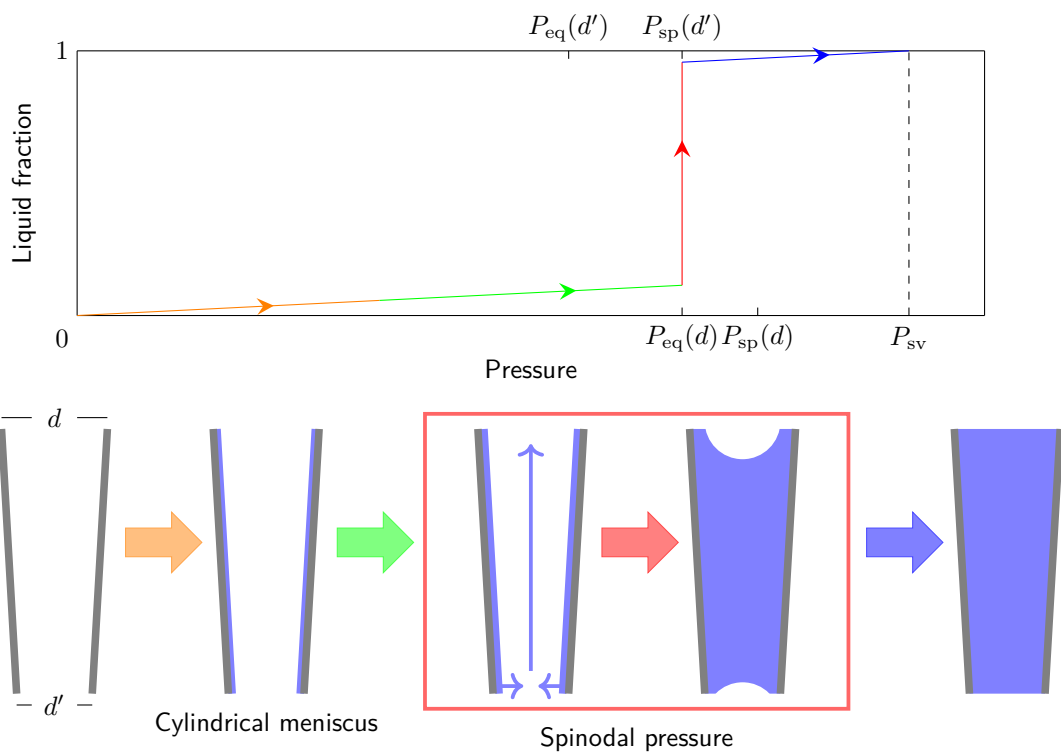
(b)

**Figure 2.3** Condensation and evaporation isotherm model of a closed cylindrical pore. (a) corresponds to the mechanisms in a straight pore whereas (b) does for a funnelled one. The corresponding processes inside the pore are illustrated below the isotherm itself. Colors of the arrows between pore states and the respecting pressure range of the graph match.

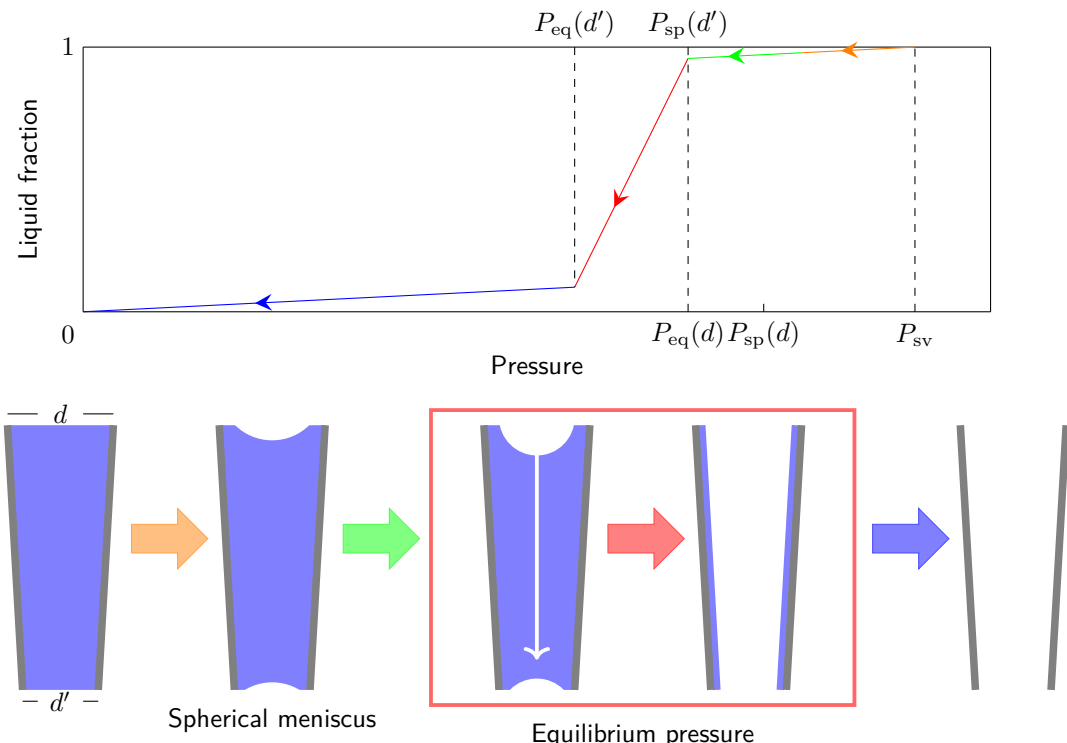


(b) Desorption isotherm. Significant is the desorption at equilibrium pressure.

**Figure 2.4** Condensation (a) and evaporation (b) isotherm of a open straight pore. The corresponding processes inside the pore are illustrated below the isotherm itself. Colors of the arrows between pore states and the respecting pressure range of the graph match.



(a) Absorption isotherm. Significant is the absorption at spinodal pressure  $P_{\text{sp}}(d') \geq P_{\text{eq}}(d)$ .



(b) Desorption isotherm. Significant is the continuous desorption at the equilibrium pressures  $P_{\text{sp}}(d)$  to  $P_{\text{sp}}(d')$ .

**Figure 2.5** Condensation (a) and evaporation (b) isotherm of a open funnelled pore. The corresponding processes inside the pore are illustrated below the isotherm itself. Colors of the arrows between pore states and the respecting pressure range of the graph match.

The menisci are spherical cap menisci as

$$P_{\text{eq}}(d) < P_{\text{sp}}(d) < P_{\text{sv}} \quad (2.4)$$

and evolve into even surfaces at saturated vapor pressure (blue).

The desorption isotherm of a straight cylindrical pore is illustrated in fig. 2.4(b). With the only difference being that spherical menisci form on both ends of the pore. The evaporation of liquid from an open, straight pore functions the same as for a closed, straight pore which is described in section 2.3.1.

Thus, condensation and evaporation occur at two different pressures yielding a hysteresis. A complete isothermal loop of condensation and evaporation is shown in fig. 2.6.

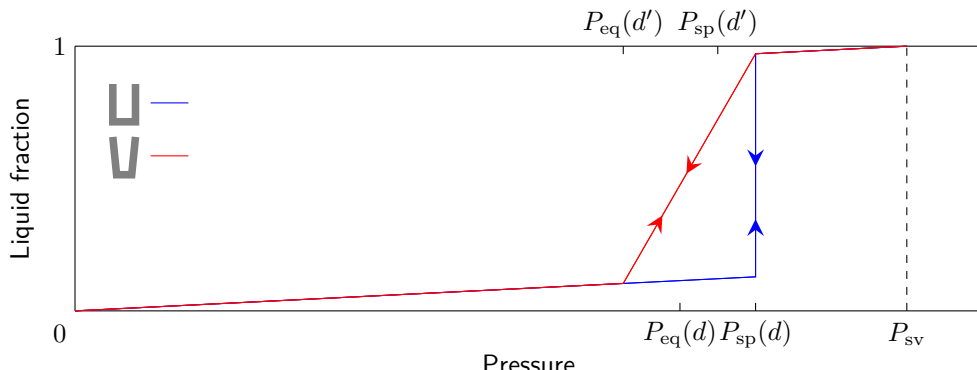
### **2.3.4 Condensation and evaporation in an open funnelled pore**

Here, a funnelled cylindrical pore that is open at both ends is regarded. In the case where the funnelling is small enough with respect to the pore's diameter for

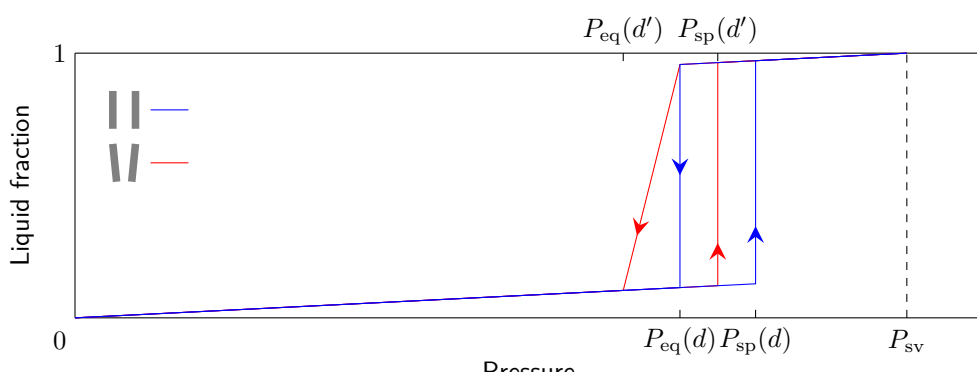
$$P_{\text{sp}}(d') \geq P_{\text{eq}}(d).$$

to hold, the pore fills abruptly at  $P_{\text{sp}}(d')$ . For stronger funnelling, the condensation branch of the isotherm shows a vertical rise, followed by a continuous increase due to the further condensation at equilibrium pressure and according to the increasing pore diameter.

In both cases, the pore empties at equilibrium pressure, starting at the large end. This makes for the same behaviour as a closed funnelled pore which has been explained in section 2.3.2.



(a) Cylindrical pore open on one end.



(b) Cylindrical pore open on both ends.

**Figure 2.6** Absorption and desorption isotherm loops for various kinds of cylindrical pores. For the funnelled pores it is  $d > d'$ .

## 2.4 Blablabla Näherung

The refractive index of a porous medium with structures in the range of the wavelength of the transmitting light can be approximated by the blablabla???. Using the porosity  $0 < \phi < 1$  as a parameter it is assumed that the effective refractive index behaves like

$$n_{\text{eff}} = n_1 (1 - \phi) + n_2 \phi$$

where  $n_{1,2}$  are the indices of the two components of which the medium is composed (for nanoporous alumina membranes in empty state the components are alumina and vacuum for example).

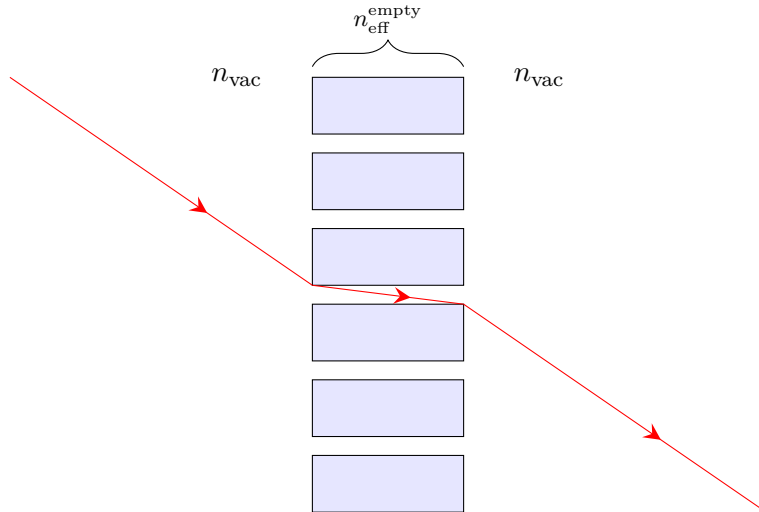


**Figure 2.7** Using the blablabla approximation for the refractive index of a nanoporous medium the transmission in its empty state is computed in section ???.

### 2.4.1 Transmission of Nanoporous Membranes in Empty and Filled State

Here, nanoporous media made of an arbitrary material - with the sole condition that  $n_{\text{mat}} > 1$  - shall be regarded in an empty and filled state. The wetting liquid's refractive index is  $n_{\text{liq}} > 1$ . The approximation section 2.4 yields the inequality

$$n_{\text{eff}}^{\text{empty}} = n_1 \cdot (1 - \phi) + n_{\text{vac}} \cdot \phi < n_1 (1 - \phi) + n_{\text{liq}} \phi = n_{\text{eff}}^{\text{filled}},$$

where

$$1 = n_{\text{vac}} < n_{\text{liq}}$$

with the refractive index of vacuum  $n_{\text{vac}}$ . Combining with the FRESNEL equations yields the transmission coefficients

$$T_{\text{empty}} = \left( \frac{2n_{\text{vac}}}{n_{\text{vac}} + n_{\text{eff}}^{\text{empty}}} \right)^2 > \left( \frac{2n_{\text{vac}}}{n_{\text{vac}} + n_{\text{eff}}^{\text{filled}}} \right)^2 = T_{\text{filled}}$$

when assuming an incident angle  $\theta_i = 0$  once again.

#### 2.4.1.1 Transmission of Empty AAM Membrane

To give an example: The transmission coefficient of an empty nanoporous alumina membrane, as used in the conducted experiments, is computed in the following way: The alumina membranes

parameters are

$$\phi = 25\% \quad (2.5)$$

$$n_{\text{Al}_2\text{O}_3} = 1,7682 \quad (2.6)$$

which make for a transmission coefficient of

$$T_{\text{Al}_2\text{O}_3}^{\text{empty}} = 0,9024. \quad (2.7)$$

## 3 Experimental results

### 3.1 Experimental approach

For the first time during the team's research on alumina membranes, systematic measurements were conducted. Due to the limited period of time, only some aspects of the membranes could be investigated in more detail. During the internship, I measured 25 membranes of 3 wafers using the experimental setup described in ???. Table 3.1 summarizes the main features of these wafers.

Victor Doebel's measurements had already shown strong dispersions in the properties of the membranes of different wafers, but also within the same wafer. Therefore, to evidence a possible systematic dispersion depending on the positions of the membranes on the wafers, the membranes are labelled according to the convention shown in fig. 3.1. Moreover, special attention was brought to the inhomogeneities on the wafers and the effect of the phosphoric acid etching used for the *barrier layer* dissolution (ref???). A processing scheme for the wafers 295 and 296, which also marks the conducted measurements, is given by fig. 3.2.

OR

Victor Doebel's initial measurements previous to this internship had already shown strong dispersions in the properties of the membranes of different wafers, but also within the same wafer. Therefore, my goal was to perform systematic measurements on alumina membranes to determine the source of these dispersions. To probe a possible dependency on the position of the membranes on the wafers, the labeling is done according to the convention shown in fig. 3.1.

Due to the limited period of time, I chose to focus on the production steps of the *barrier layer* dissolution and the pore diameter reduction by atomic layer deposition. During the internship, I measured 25 membranes of 4 wafers using the experimental setup described in ???. Table 3.1 summarizes the main characteristics of these wafers. A processing scheme for the wafers 295 and 296, which also marks the conducted measurements, is given by fig. 3.2.

At first glance, resolving the bad open pore issue seems as easy as simply increasing the membranes' floating time during the *barrier layer* dissolution. On second thought though, a problem comes up: Figure 3.11 clearly states that some pores open before others. Therefore, these open pores are infiltrated by phosphoric acid which starts etching the pore from the inside increasing its diameter. This results in a broadening pore diameter distribution on the membrane caused by the *barrier layer*

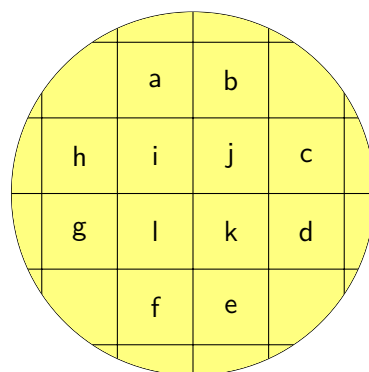


**Figure 3.1** Convention used to assign membrane depending on their position on the wafer.

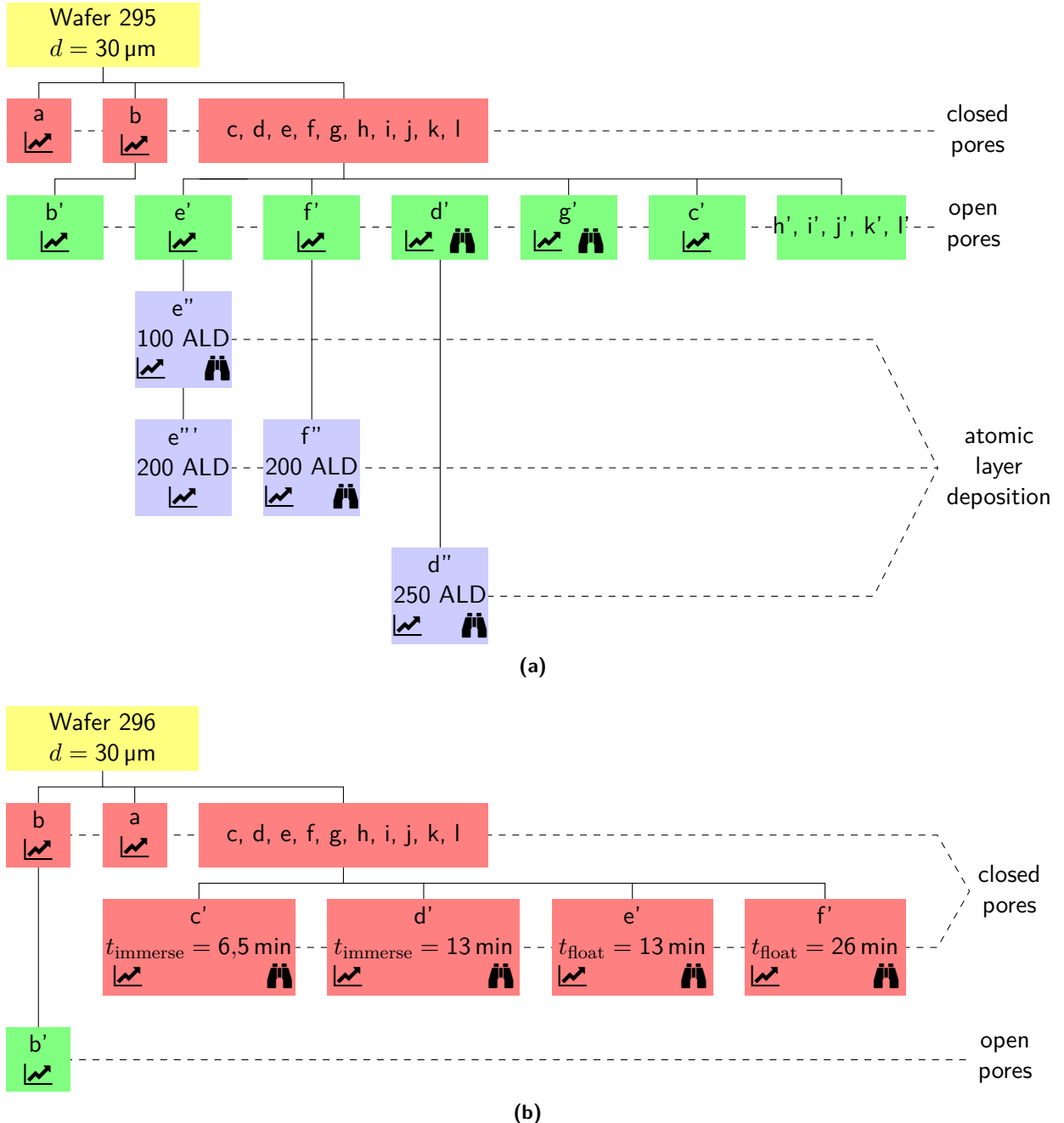


**Figure 3.2** Wafer 295 and 296 processing scheme. While a signifies a recorded isotherm, the means MEB pictures have been taken. Red marks pores closed on one end, green pores open on both ends. The processed wafers are immersed in phosphoric acid for  $t_{\text{immerse}}$  or floated on for  $t_{\text{float}}$ .

**Table 3.1** Wafer specifications. The wafers thickness  $l_{\text{pore}}$ , floating time  $t_{\text{float}}$  of the *barrier layer* dissolution process and pore diameter dispersion  $\Delta d_{\text{pore}}^{\text{MEB}}$  measured by electron beam microscopy are noted. The latter two parameters apply to the open pore membranes of the respective wafer.

Wafer	$l_{\text{pore}}$ [μm]	$t_{\text{float}}$ [min]	$\Delta d_{\text{pore}}^{\text{MEB}}$ [nm]
292	60	36+4	-
294	60	33	-
295	30	35 (38 for b)	7
296	60	40	-

dissolution process.

As mentioned in ???MEMBRANE PRODUCTION, milky aspects occur at some point of the floating. Same as for spinodal condensation in the membranes, the filling of the opening pores with acid is assumed to cause light scattering and can therefore be linked to these milky aspects. Proof of this theory is the SEM image taken of a membrane that has been floated until the milky aspects appeared. Shown in fig. 3.3, the image confirms the semi open state of the membrane. As the milky aspects last for about

$$t_{\text{milky}} = 3 \text{ min}$$

and the etch rate of phosphoric acid on alumina is expected to be

$$e = 1 \frac{\text{nm}}{\text{s}},$$

the barrier layer dissolution process should cause an increase of the pore diameter dispersion of

$$\Delta d_{\text{pore}} = 6 \text{ nanom}.$$

This is quite dramatic regarding that the pore diameter distribution of a closed pore limited to about 10 nm ??? PROOVE!. Therefore, this increase should be obvious on the comparison of the evaporation branches of a closed pore membrane with an equivalent open pore membrane. Using section 3.2.2 as an example does not confirm these expectations which leads to the suspicion that the etch rates parallel to the pore axis  $e_{\parallel}$  and perpendicular to the axis  $e_{\perp}$  are different.

To avoid this, one might think of immersing the membrane in order to fill every pore at the same time. While the pores would be widened during the whole *barrier layer* dissolution process then, the distribution remained unchanged. However, the etch rate of phosphoric acid on alumina is expected to be approximately

$$e = 1 \frac{\text{nm}}{\text{min}}$$

which makes for a pore diameter increase of infiltrated pores of

$$\dot{\Delta}d_{\text{pore}} = 2 \frac{\text{nm}}{\text{min}}.$$

From SEM images the thickness of the *barrier layer* has been determined to be

$$d_{\text{barrier-layer}} = 30 \text{ nm},$$

so to open the pores at least 15 min translating to a pore diameter increase of

$$\Delta d_{\text{pore}} = 30 \text{ nm}.$$

As the aim is rather to produce membranes with pore diameters  $d_{\text{pore}} < 10 \text{ nm}$ , the pure immersion becomes a backup plan.

Instead, I developed the idea of a combination of floating to decrease the thickness of the barrier layer and immersion to do the final pore opening.

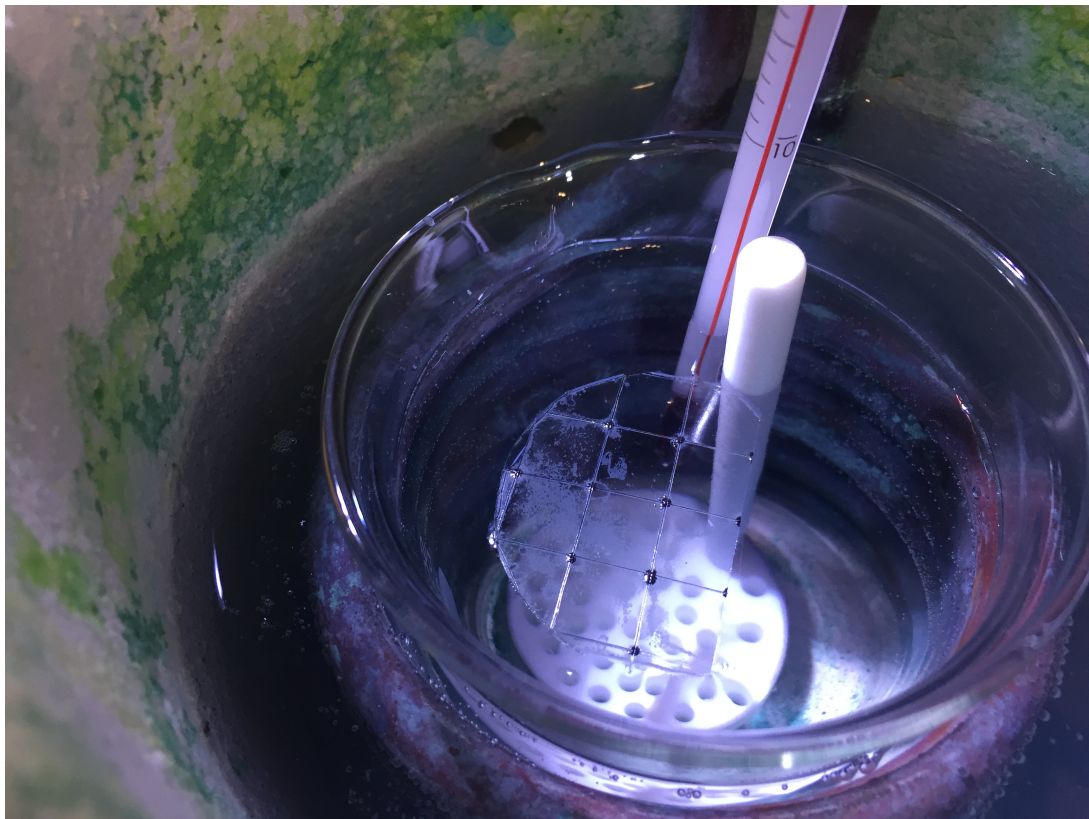


**Figure 3.3** SEM image of a membran floated on phosphoric acid until the appearance of milky aspects.

## 3.2 Membrane structure analysis

### 3.2.1 Isotherm of an open pore membrane

To start with, an isotherm of an open pore membrane is compared to theory. According to section 2.3, expectations are that condensation and evaporation occur at pressures smaller than the saturated vapor pressure  $P_{sv}$ . Moreover, the condensation occurring at spinodal pressure  $P_{sp}$  and the evaporation at  $P_{eq}$  implies a hysteresis. For the transmission measurement, two drops of transmission corresponding to condensation and evaporation are expected. Furthermore, the transmission should increase for the filled membrane in respect to its empty state.

Section 3.2.1 shows the measured isotherm of open pore membrane 296b'. As expected, condensation and evaporation occur at pressures

$$P_{rel,eq}^{296b'} < P_{rel,sp}^{296b'} < P_{rel,sv}$$

yielding a hysteresis. The dashed lines in section 3.2.1 mark the average condensation and evaporation pressures of the isotherm. For their determination, the steepest point of the liquid fraction graph is sought, which corresponds to the minima of the transmission signals as expected. Converting these to diameters using KELVIN equation yields

$$\begin{aligned} d_{pore}^{296b'}(P_{rel,sp}^{296b'} = 0,956) &= 44,4 \text{ nm}, \\ d_{pore}^{296b'}(P_{rel,eq}^{296b'} = 0,925) &= 51,3 \text{ nm}, \end{aligned}$$

which makes for reasonable results. Furthermore, the transmission behaves according to theory in regard of the filled transmission in filled state being stronger than for the empty state. (COMPARE TO SEM OF 296e???)

By theory, the condensation and evaporation are expected to be vertical. The inclination of the two isotherm branches is explained as follows. Evaporating at equilibrium pressure leads to an inclined

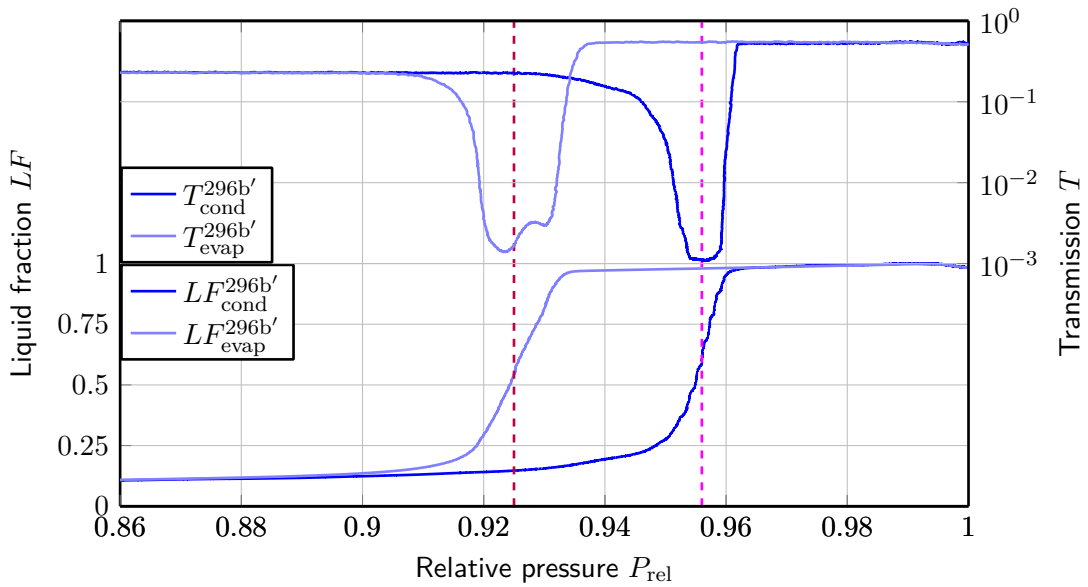


**Figure 3.4** Measurement results of open pore membrane 296b'. The dashed lines mark the average condensation and evaporation pressures.

isotherm branch if there are either funnelled pores or the pores' diameters are distributed. On the other hand, condensation at spinodal pressure in weakly funnelled cylindrical pores (compare section 2.3.4) only shows an inclination if the pore sizes are distributed. At this point, the funnelling could be excluded to explain the observed isotherm. SEM images of various open pore membranes show a difference between the diameters of the solution and the aluminum side, which implies the presence of the pores' funnelling. Figure 3.5 shows the respective images of membrane 295g', supporting the assumption of pore funnelling.

### 3.2.2 Isotherm of a closed pore membrane

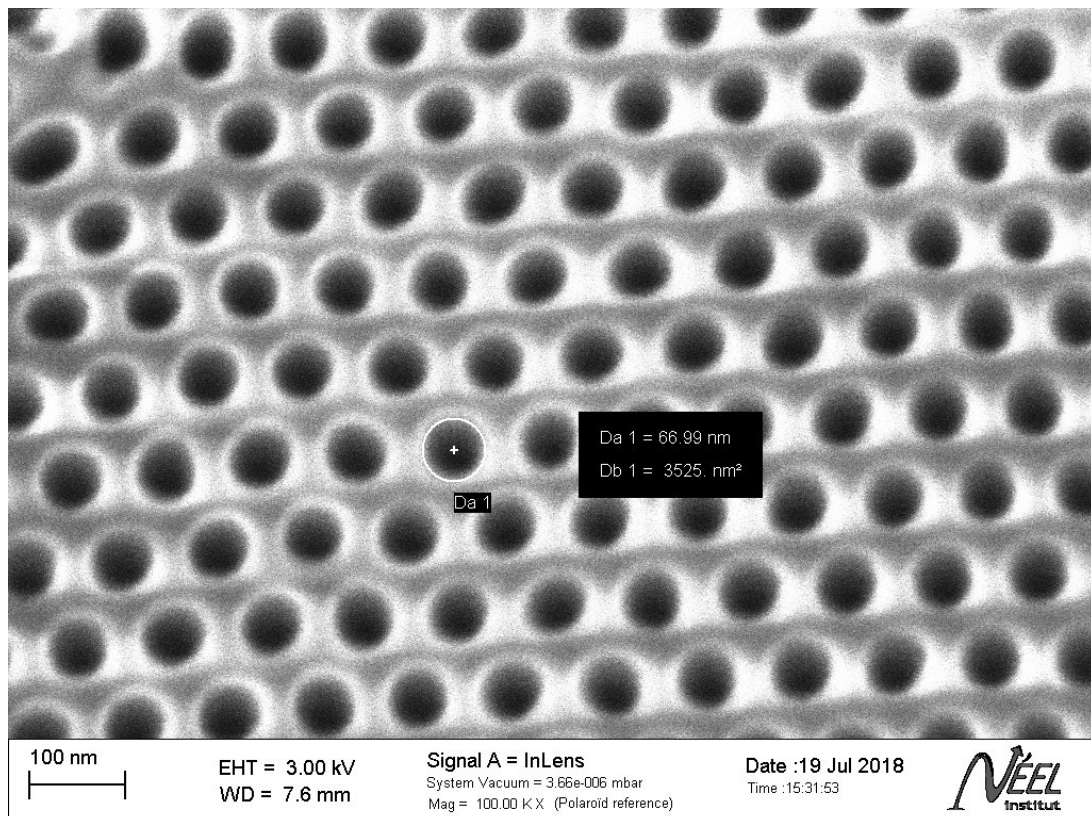
Moving on to a closed pore membrane, according to section 2.3, no hysteresis is expected as both, condensation and evaporation occur at equilibrium pressure

$$P_{\text{eq}} < P_{\text{sv}}$$

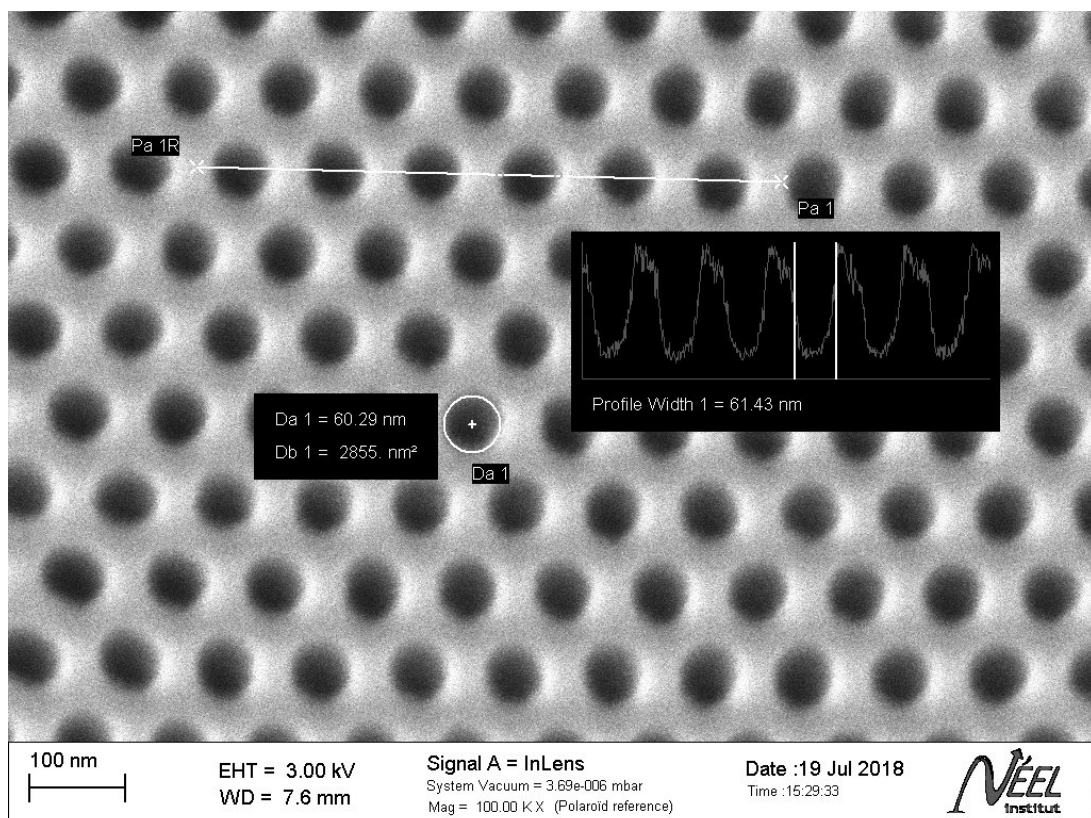
and should therefore be superimposed with the evaporation branch of an equivalent open pore membrane. For the transmission signal, the same behaviour as for the open pore membrane is expected: Two drops at condensation and evaporation respectively and a higher value in the filled state than in the empty state.

Section 3.2.2 shows the isotherm of a closed pore membrane 296b along with an open pore membrane 296b'. First, condensation indeed shifts to lower pressures for the closed pore membrane. Moreover, the evaporation branch is also shifted to lower pressures. As will be explained in ???, this is due to the pore widening upon the *barrier layer* dissolution process. As for the transmission, the drops' positions correspond to those of the volumetric isotherm's rises and filled state transmission is stronger than empty state transmission. However, the drastic increase in magnitude of the transmission signal upon the pore opening is not clear.

That the hysteresis does not disappear is assumably due to intra pore corrugations. The latter vary the equilibrium pressure  $P_{\text{eq}}(d_{\text{pore}})$  along the pore's length, which then causes the hysteretic behaviour. The phenomenon has been observed and explained this way by various experimentators REF???.



(a)



(b)

**Figure 3.5** SEM images of membrane 295g' implying the pores' funnelling. The pores on the solution side (a) show bigger diameters than those on the aluminum side (b).

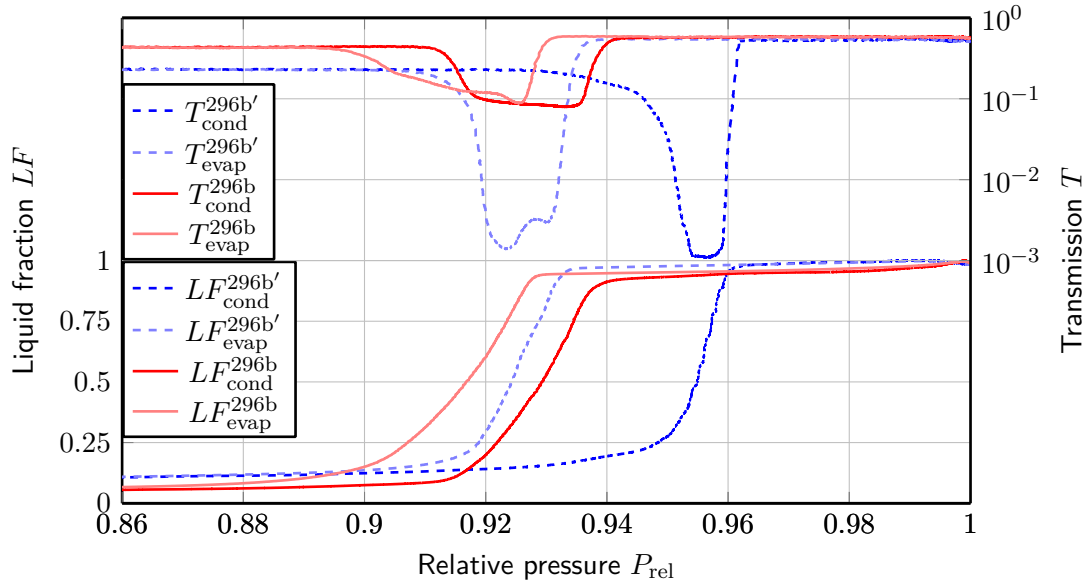


**Figure 3.6** Measurement results of closed pore membrane 296b in comparison to the open pore membrane 296b'.

### 3.2.3 Measurement reproducibility

To check the reproducibility of the isotherm measurements, membranes were measured multiple times. Section 3.2.3 shows four consecutive measurements for the same open pore membrane 292c and one more independent measurement ( $LF_{\text{cond/evap}}^{292c,5}$ ). All the curves are close to superimposed. The biggest offset occurs before the condensation at spinodal pressure. As this part of the isotherm is not so important for the analysis, one can say that the volumetric measurements are very reproducible.

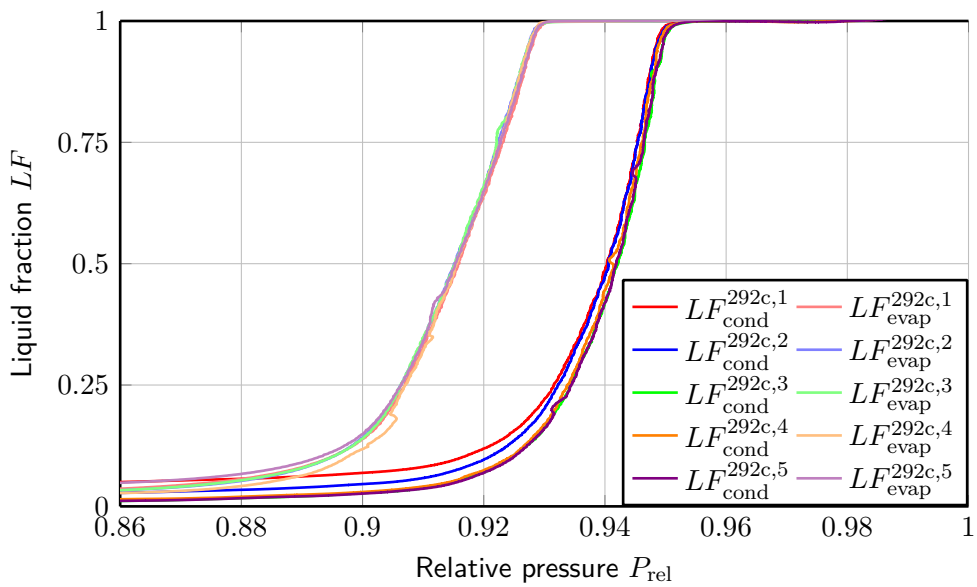


**Figure 3.7** Reproducibility test comparing multiple isotherms measured for the same membrane 292c.

ADD OPTICAL MEASUREMENT??? not possible for 292c, would have to use other membranes with a maximum of two consecutive measurements...

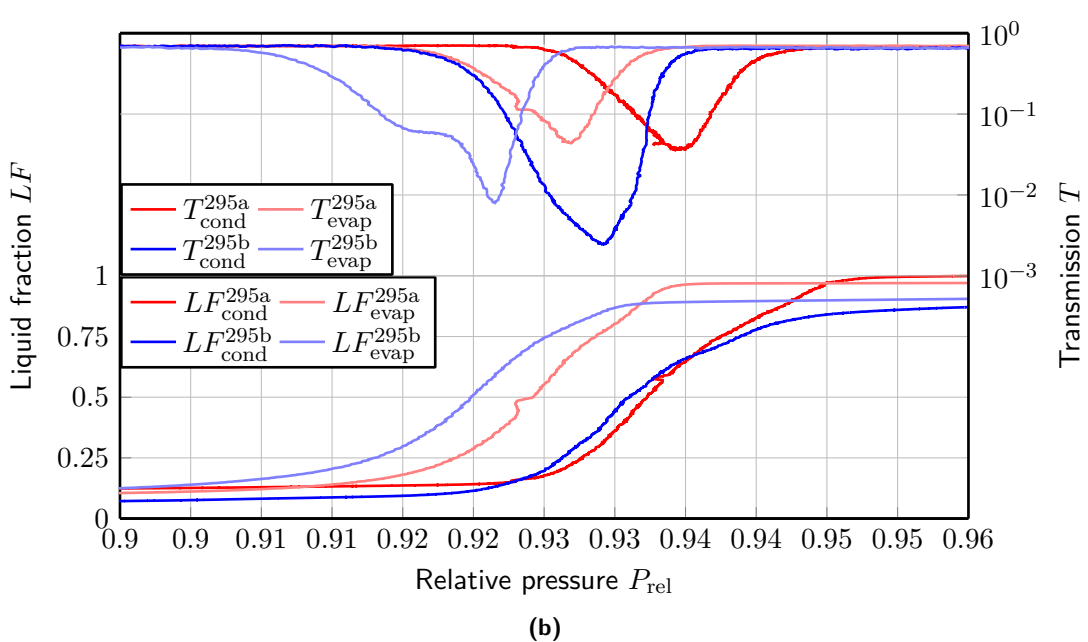
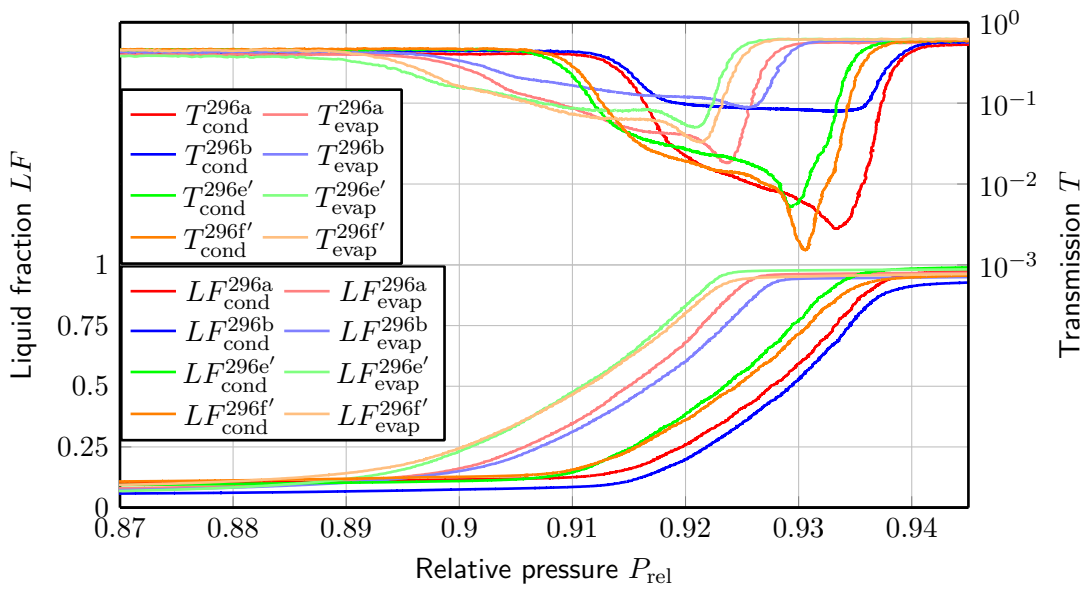


**Figure 3.8** Comparison of closed pore membranes of one wafer. (a) compares membranes of wafer 296 while fig. 3.8(b) deals with 295.

### **3.2.4 Inhomogeneities on one wafer**

To start with, the wafers shall be tested for inhomogeneities. Therefore, isotherms of one wafer's membranes, which are in the same technical state, and have undergone exactly the same treatments, are compared. This is done for both: Closed pore membranes and open pore membranes. Because opening the membranes' pores involves one more production step, here, closed pore membranes are regarded first.

Figure 3.8 shows a comparison of closed pore membranes for wafer 295 and 296. Even though the membranes 296e' and 296f' had already been treated using phosphoric acid at the time of the measurements, the pores are still closed as will be explained in ??.

While for both wafers the overall shape of the different membranes' measurements matches, with one exception being membrane 295c, they are distributed along a short distance of the  $P_{\text{rel}}$ -axis. As long as the shapes and also the size of the hysteresis of the volumetric isotherm match, this can be explained by differing pore size distributions. Membrane 295c is not analysed at this point, as it will be dealt with in detail in ??????. Unclear at this point is the extreme variation in magnitude of the transmission signal between the membranes (compare 296f' and 296b).

In conclusion, to measure the effect of treatments on a given membrane, before and after measurements are necessary. It is not enough to measure one membrane representatively for multiple membranes in the same state.

### **3.2.5 Defects**

All in all, the conducted measurements yield great results. The measured isotherms go along with the model introduced in section 2.3 and are reproducible. The inhomogeneity on a given wafer is bearable???

Nevertheless, pore defects and dispersions were detected. First, there is the pore size distribution. To estimate its broadness, SEM images are analyzed in 295g???. Next, the funnellization and the corrugation must be mentioned. Both cause intra pore diameter variations that cause inclined isotherms, even for a single pore. Last, bad open pores were detected during the measurements. This problem will be discussed in the following section, as its examination leads to valuable, relevant results.

## **3.3 The problem of pore opening**

### **3.3.1 Bad open pores**

Victor Doebel's measurements before my internship revealed membranes with bad open pores. The term *bad open pores* refers to a membrane that has been floated on phosphoric acid for the *barrier layer* dissolution not long enough to completely open the pores. ???TIKZ IMAGE??? As a result some pores remain closed whereas others have constricted openings and some are fully open. Section 3.3.1 shows the comparison of closed pore membrane 294cp and membrane 294op with bad open pores. The assumption is derived from the isotherm in the following way: By theory, the condensation branch should be shifted towards higher pressure for open pores in respect to closed pores. While this is the case for membrane 294op's end of the condensation rise, it still starts at the same pressure as the condensation of the closed pore membrane which by theory condenses at equilibrium pressure. Moreover, the evaporation of 294op is superimposed with the one of 294cp. While this is expected by theory, it rules out the possibility of an increase in funnellization or corrugation causing the broader condensation branch of the open pore membrane. The only possible explanation for the observed behaviour is a population of open pores alongside one of closed pores on the membrane. In this case some pores start filling at equilibrium pressure, wheras others fill at higher spinodal pressures

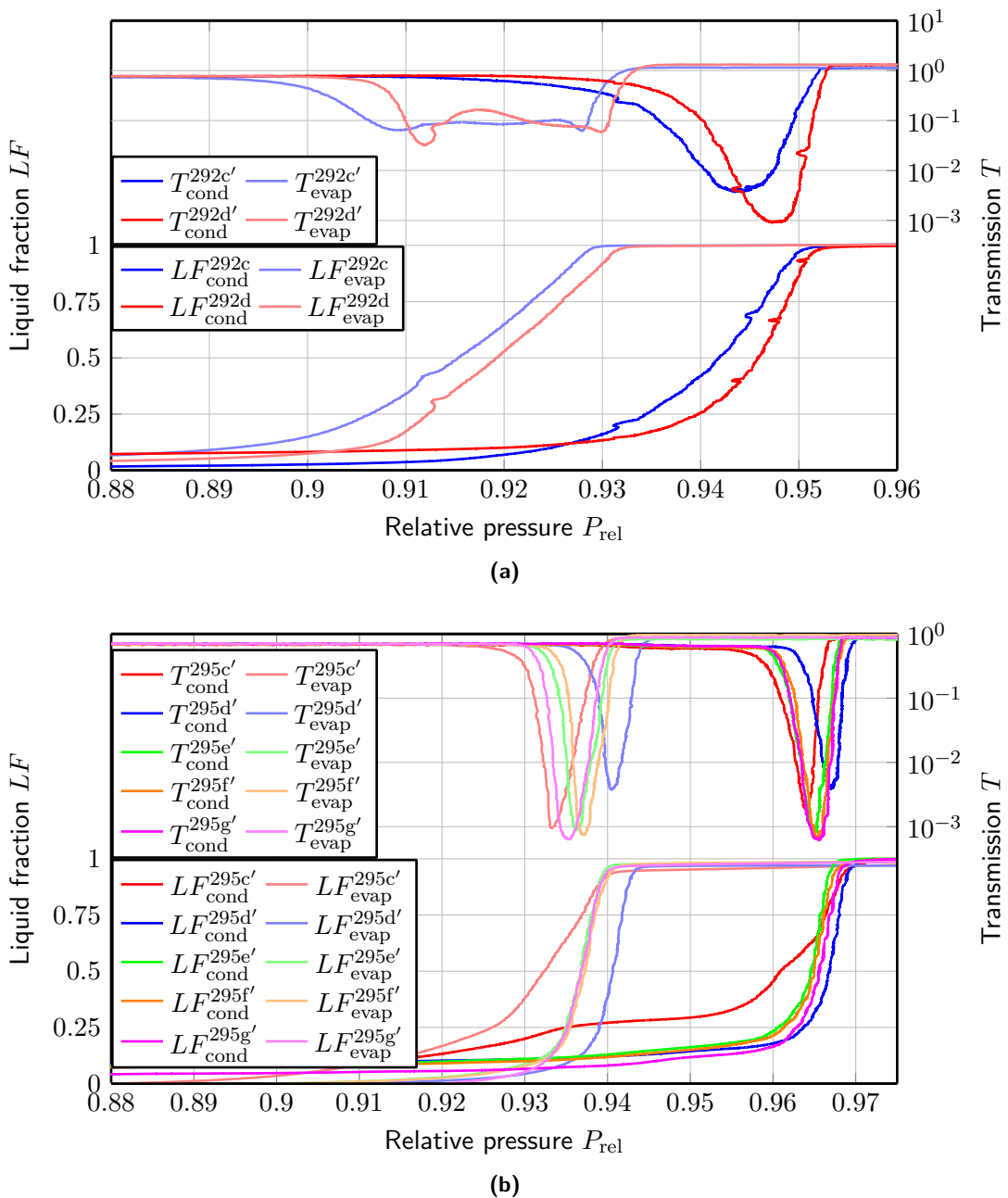


**Figure 3.9** Comparison of open pore membranes of one wafer. (a) compares membranes of wafer 292 while fig. 3.9(b) deals with 295.

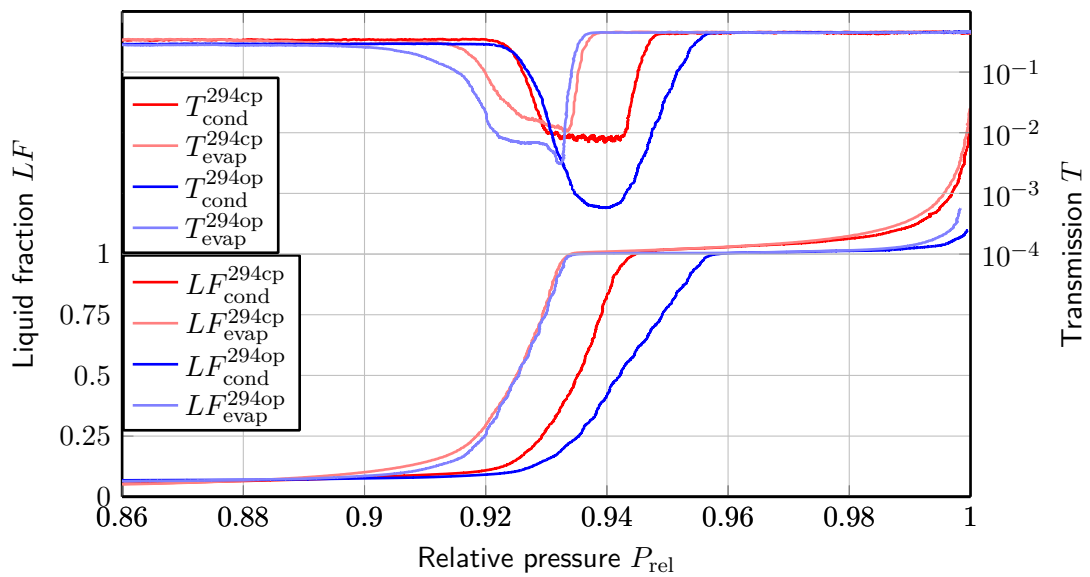


**Figure 3.10** Bad open pores illustrated by the comparison of a closed pore isotherm and a open pore isotherm of membrane 294a.

depending on the size of the pore opening on the aluminum side. independently, SEM images of the membrane confirm the assumption of bad open pores as shown in fig. 3.11.

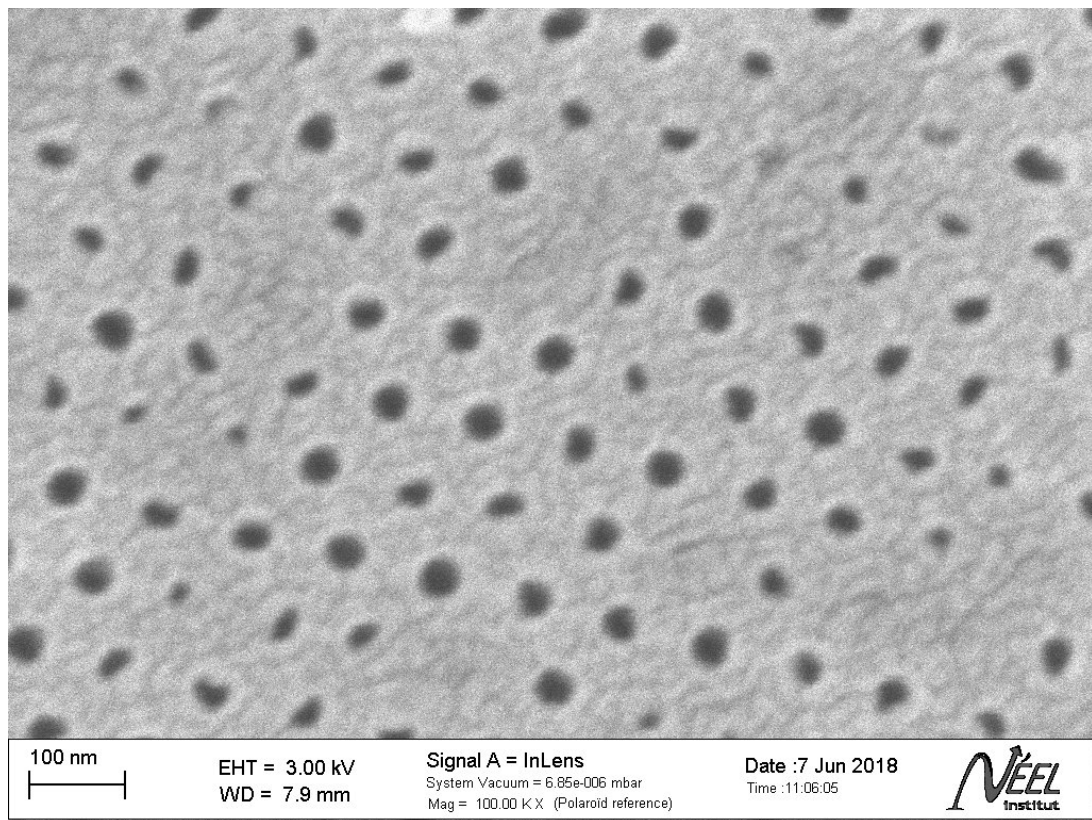


**Figure 3.11** SEM image confirming the bad open pores of membrane 294op.

## Bibliography

[Cd15] Universität Konstanz: Corporate Design Manual. Universität Konstanz, (2015)